




JGR Space Physics

RESEARCH ARTICLE

10.1029/2018JA026303

Formation of Asymmetric Electron Acoustic Double Layers in the Earth's Inner Magnetosphere

Ajay Lotekar¹ , Amar Kakad¹ , and Bharati Kakad¹ 

¹Indian Institute of Geomagnetism, New Panvel (West), Navi Mumbai, India

Key Points:

- Fluid simulation is performed to study the formation and evolution of asymmetric solitary waves in the Earth's inner magnetosphere
- Ponderomotive force modulates the symmetric solitary wave pulses into the asymmetric pulses of double layers
- Electron acoustic shock-type waves play an important role in the formation of electron acoustic double layers

Supporting Information:

- Supporting Information S1
- Movie S1
- Movie S2

Correspondence to:

A. Lotekar,
 ablotekar@gmail.com

Citation:

Lotekar, A., Kakad, A., & Kakad, B. (2019). Formation of asymmetric electron acoustic double layers in the Earth's inner magnetosphere. *Journal of Geophysical Research: Space Physics*, 124, 6896–6905. <https://doi.org/10.1029/2018JA026303>

Received 19 NOV 2018

Accepted 5 AUG 2019

Accepted article online 17 AUG 2019

Published online 30 AUG 2019

Abstract The Van Allen Probes have observed both symmetric and asymmetric bipolar electric field structures in the Earth's inner magnetosphere. In general, the symmetric bipolar structures are identified as electron-phase space holes, whereas the asymmetric structures are interpreted as electron acoustic double layers (EADLs). The generation mechanism of these EADLs is not entirely understood yet. We have modeled the EADLs observed on 13 November 2012 by Van Allen Probe-B. We performed a fluid simulation of the EADLs and tracked their formation and evolution in the simulation. We found that the localized depletion and enhancement in the electron populations act as a perturbation to excite the symmetric bipolar electron acoustic solitary waves, which later evolve into the EADLs. The Ponderomotive force is found to be the main driver behind transformation of the symmetric electron acoustic solitary waves to EADLs via formation of the electron acoustic shocks.

1. Introduction

The Van Allen Probes have demonstrated the occurrence of a wide variety of electric field structures associated with the various plasma boundaries in the terrestrial inner magnetosphere (Ergun et al., 2015; Malaspina et al., 2018; Mozer et al., 2015). Most of these structures have large electric field component along the local magnetic field, which makes them electrostatic in nature. Such electrostatic solitary wave structures mostly include electron acoustic solitary waves (Vasko et al., 2017), electron acoustic double layers (Dillard et al., 2018; Mozer et al., 2015; Vasko et al., 2017), electron-phase space holes (Mozer et al., 2015), relativistic electron double layers, and strong double layers (Malaspina et al., 2014).

A careful scrutiny of observations suggests that the electric field structures associated with plasma boundaries in the inner magnetosphere are bipolar with either symmetric and asymmetric parallel electric field as recently pointed out by Vasko et al. (2017, 2018). Earlier observational studies demonstrated that the symmetric electrostatic solitary waves correspond to electron holes (Matsumoto et al., 1994; Cattell et al., 2005; Ergun et al., 1998; Mozer et al., 2015). Vasko et al. (2017) reported intense asymmetric solitary wave pulses (durations ≥ 1 ms) propagating along magnetic field lines with a velocity close to the thermal velocity of 100 to 200 eV electrons in the Earth's inner magnetosphere. These structures were identified as electron acoustic double layers (EADLs) and concluded to have the convergent electric field configuration. Vasko et al. (2017) adopted the small-amplitude KdV theory to suggest a scenario for formation of the EADLs. Recently, Vasko et al. (2018) demonstrated the mechanism of formation of EADLs observed in association with whistler waves. However, the generation mechanism of EADLs in the absence of whistler waves is still an open question. Fu et al. (2016) made an attempt to generate EADLs by performing the particle-in-cell simulation but reported negative results.

In this paper, we investigate the generation mechanism of EADLs in the absence of whistler waves by using localized density perturbations of electrons. Using fluid simulations, we have modeled the EADLs observed by Van Allen Probe-B. We also examined the propagation characteristics of these EADLs to address their sustainability in the space. The paper is organized as follows: Formulation of the model and its validation with the observations are given in section 2. The fluid simulation of the EADLs is elaborated in section 3, and their generation mechanism is discussed in section 4. We conclude this paper in section 5.

2. Nonlinear Fluid Model of EADLs

We considered the observation of the EADLs by Van Allen Probe-B on 13 November 2012 (Vasko et al., 2017). The ambient parameters required for the simulation are chosen based on the data analysis presented

Table 1

The Ambient Electron Parameters and Solitary Wave Characteristics Observed on 13 November 2012 by RBSP-B in the Inner Magnetosphere Are Given in the Third Column

No.		Observation	Theory	Simulation
1	n_{e0} (cm ⁻³)	~4.2	4.2	4.2
2	n_{h0} (cm ⁻³)	~3	4.15 to 2.4	2.52
3	n_{c0} (cm ⁻³)	Free parameter	0.05 to 1.8	1.68
4	T_h (eV)	~100 to 10,000	200	200
5	T_c (eV)	~<100	2	2
6	E (mV/m)	~ -20 to 35	-128 to 128	6.50
7	V (km/s)	~1,000 to 6,000	5,408 to 6,857	6,561

Note. Details of these observations are given in Vasko et al. (2017). The fourth and fifth column respectively gives the corresponding ambient parameters taken as an input for the theory and the simulation.

by Vasko et al. (2017) and they are listed in Table 1. A careful examination of electron densities observed by Helium, Oxygen, Proton, and Electron (HOPE) detector (Funsten et al., 2013) during the observation of EADLs reveals that the total electron density (n_{e0}) is ~4.2 cm⁻³ and the hot electron density (n_{h0}) is ~3 cm⁻³ (refer to Figure 2a of Vasko et al., 2017). One also expects some population of cold electrons (below few electronvolts) of ionospheric origin at the observation location in the inner magnetosphere. Because the cold electrons play an important role in the excitation of electron acoustic modes in plasmas (Watanabe & Taniuti, 1977), we have considered cold electrons in our model. However, the measurement of cold electron density is not available because of the spacecraft charging; therefore, we treat the cold electron density (n_{c0}) as a varying parameter by choosing a range of 0.05–1.8 cm⁻³, that is from 1–40% of the total electron density.

While deriving the KdV equation for small-amplitude waves, Vasko et al. (2017) neglected the inertia of electrons above 100 eV and derived the modified Boltzmann distribution for the density of these electrons. However, we have retained the inertia of both cold and hot electrons in our model. The ions are assumed to have uniform density distribution, and for simplicity, their dynamics is neglected. This assumption is justified by the fact that the large mass ratio between ion and electron prevents ions from contributing significantly to the electron acoustic waves (Watanabe & Taniuti, 1977). For the electrostatic conditions the plasma system is governed by the following fluid equations,

$$\frac{\partial n_s}{\partial t} + \frac{\partial(n_s v_s)}{\partial x} = 0 \quad (1)$$

$$\frac{\partial v_s}{\partial t} + v_s \frac{\partial v_s}{\partial x} + \frac{1}{m_s n_s} \frac{\partial p_s}{\partial x} - \frac{q_s}{m_s} E = 0 \quad (2)$$

$$\frac{\partial p_s}{\partial t} + v_s \frac{\partial p_s}{\partial x} + \gamma p_s \frac{\partial v_s}{\partial x} = 0 \quad (3)$$

where $s = c, h$ corresponds to cold and hot electrons, respectively. n_s , v_s , and p_s are density, velocity, and pressure of the species s , respectively. The mass and charge of given species is respectively referred as m_s and q_s . Here, γ is an adiabatic index, which is in general considered to be equal to one for hot electrons [Sagdeev, 1966]. However, it may be different from one for non-Maxwellian plasma (Vasko et al, 2017). In this study, we have assumed the same adiabatic equation of state with $\gamma = 3$ for all the species as we deal with the one-dimensional plasma system. In such a case, the choice of $\gamma = 3$ appears to be appropriate as particles have essentially 1 degree of freedom along the wave propagation direction (Kakad et al., 2019). In such a case, the equations above are coupled with the following Poisson's equation

$$\epsilon_0 \frac{\partial E}{\partial x} = e(n_0 - n_c - n_h). \quad (4)$$

The electric field E can be expressed in terms of an electrostatic potential with the relation, $E = -\partial\phi/\partial x$. At the equilibrium, plasma follows quasi-neutrality, under which the equilibrium plasma density is $n_0 = n_{c0} + n_{h0}$. Here, n_{c0} and n_{h0} are cold and hot electron density at the equilibrium, respectively.

As a first step, we performed the fully nonlinear Sagdeev pseudo-potential analysis (Sagdeev, 1966) to obtain the arbitrary solitary wave solutions. This analysis involves transformation of the above set of equations to a frame moving with the wave by considering $\xi = x - Vt$, where V is the velocity of the solitary wave structure. We solve the set of equations (1)–(3) following Sagdeev's pseudo-potential approach and obtain the electron densities as (Kakad et al., 2016; Olivier et al., 2015)

$$n_s = \frac{n_{s0}A_{s+}}{2B_s} \left(1 + \frac{2\phi}{m_s A_{s+}^2} \right)^{\frac{1}{2}} - \frac{n_{s0}A_{s-}}{2B_s} \left(1 + \frac{2\phi}{m_s A_{s-}^2} \right)^{\frac{1}{2}} \quad (5)$$

where $A_{s\pm} = V \pm B_s$ and $B_s = \sqrt{3T_s/m_s}$.

Substituting the densities of cold and hot electrons from equation (5) in (4), and integrating Poisson's equation gives the following energy integral:

$$\frac{1}{2} \left(\frac{\partial\phi}{\partial\xi} \right)^2 + \psi(\phi, V) = 0 \quad (6)$$

where

$$\psi(\phi, V) = \phi + \sum_s \frac{m_s n_{s0} A_{s+}^3}{6B_s} \left[1 - \left(1 + \frac{2\phi}{m_s A_{s+}^2} \right)^{\frac{3}{2}} \right] - \sum_s \frac{m_s n_{s0} A_{s-}^3}{6B_s} \left[1 - \left(1 + \frac{2\phi}{m_s A_{s-}^2} \right)^{\frac{3}{2}} \right] \quad (7)$$

Equation (6) yields symmetric bipolar electron acoustic solitary wave (EASW) and EADL solutions for the observed electron parameters listed in Table 1. A specific value of T_c and T_h is chosen from the observations as an input to this theoretical model. As mentioned earlier, we have treated the n_{c0} as a free parameter within its range and accordingly used the hot electron density by incorporating the quasi-neutrality condition, that is, $n_{h0} = n_0 - n_{c0}$. We examined the complete range of velocities and amplitudes of EASW and EADL solutions that are supported for given input parameters. For given parameters, equation (6) supports two oppositely propagating (i.e., with $\pm V$) EASW or EADL pulses with indistinguishable characteristics. Here positive sign of V indicates the propagation of EASW or EADL pulse along the direction of magnetic field, whereas negative sign indicates their propagation antiparallel to the magnetic field. For a given value of n_{c0} range of velocity (i.e., V_{\min} and V_{\max}) of EASWs is shown in Figure 1a. The maximum electric field associated with the EASWs and EADLs traveling with $\pm V_{\max}$ is depicted in Figure 1b. We noticed that the model supports EADL solutions with positive and negative electric field amplitudes for a certain range of n_{c0} . This region is marked in Figure 1 (magenta and yellow color). The observed range of the electric field amplitude (E_{obs}) and the phase velocity (V_{obs}) of EADLs as given by Vasko et al. (2017) are marked with the shaded light green color in Figure 1. It is seen that the range of amplitudes and phase velocities predicted by theory are comparable with the observations for the particular range of cold electron density. The solitary waves predicted by the Sagdeev's pseudo-potential approach have negative electrostatic potential or, alternatively, convergent electric field configuration. It should be noted that the Sagdeev pseudo-potential approach gives solitary wave solutions supported for these ambient plasma parameter; however, it does not give any information about their evolution.

Vasko et al. (2017) have discussed the observations of EADLs propagating in directions both parallel and antiparallel to the magnetic field. The reported EADLs are asymmetric solitary waves with convergent electric field configuration that is similar to convergent configuration of EADLs predicted by the Sagdeev's pseudo-potential method. It means that the observed EADLs are indeed associated with the electrostatic potential structures with negative amplitudes. This particular aspect is confirmed by performing the fluid simulation of EADLs and it is detailed in section 3.

3. Fluid Simulation of EADLs

We simulate the Earth's inner magnetospheric plasma as an infinite, collisionless, and unmagnetized plasma system consisting of cold electrons, hot electrons, and ions. As mentioned in section 2, we treated both electron populations as mobile while ions are considered as a uniform immobile charge-neutralizing background. We consider only the nonlinear electrostatic waves propagating parallel to the magnetic field. Therefore, the dynamics of each species is governed by the multifluid equations of continuity (equation 1), momentum (equation 2), and equation of state (equation 3), and the Poisson equation (equation 4) as given

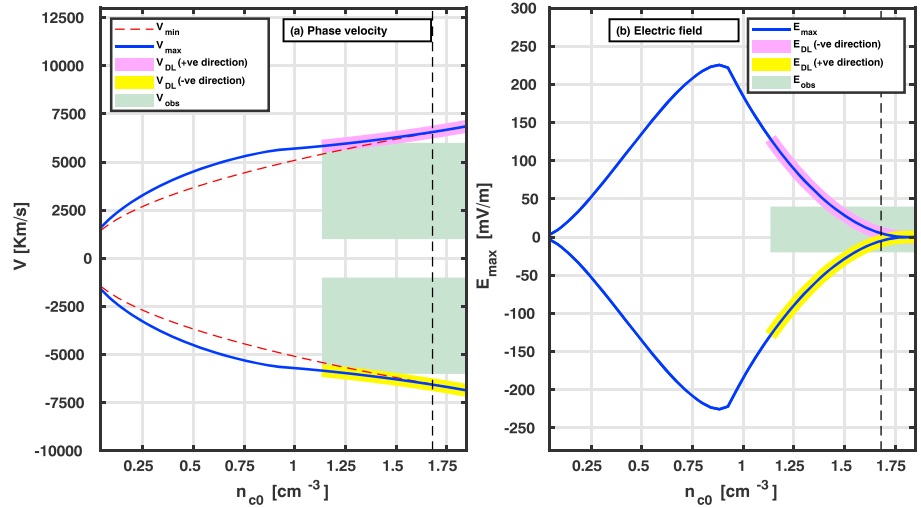


Figure 1. The variation of (a) minimum (V_{\min}) and maximum (V_{\max}) phase velocity, and (b) maximum electric field (E_{\max}) of the solitary waves supported by theory as a function of cold electron density, n_{c0} . The observed range of the electric field amplitude (E_{obs}) and the phase velocity (V_{obs}) of the electron acoustic double layers (from Figures 2 and 3 of Vasko et al., 2017) are marked with the green color. The negative and positive polarity double layer (DL) amplitude and their velocities are respectively marked by the magenta and yellow color. The vertical dotted line indicates the value of input parameter used in the simulation.

in section 2. From the nonlinear fluid model, we understand that the plasma supports propagation of EASWs and EADLs parallel and antiparallel to the magnetic field for the chosen observed ambient parameters in the inner magnetosphere. However, this model gives the stationary EASW and EADL solutions, which does not give information on how these structures are formed from an initial perturbation. We particularly focus on the generation mechanism of the observed EADLs. Thus, we carried out fluid simulations to understand the formation and evolution of EADLs in the system. The input parameters considered for the one-dimensional fluid simulation are given in Table 1, which are within the range of the background plasma parameters observed by the Van Allen Probes. These input parameters are the same as those for the nonlinear theory except for the cold electron density. We consider $n_{c0} = 1.68 \text{ cm}^{-3}$ in the simulation. This is chosen because near this cold electron concentration the theory predicts the EADLs with electric field amplitudes comparable to the observations (see Figure 2 of Vasko et al., 2017).

In the development of the fluid code, equations (1)–(4) were solved by using numerical schemes discussed in Kakad et al. (2013, 2014, 2016, 2019) and Kakad and Kakad (2016). The fluid simulation was performed in a one-dimensional system with periodic boundary conditions. Initially, the background electron densities were superimposed by considering the following localized Gaussian-type perturbation as

$$n_s = n_{s0} + \Delta n_s \exp \left[- \left[\frac{x - x_c}{l_0} \right]^2 \right] \quad (8)$$

where $\Delta n_c = -\Delta n_h$ and l_0 denote the amplitude and width of the superimposed density perturbations, and x_c is the center of the simulation system.

We perform the simulation with $\Delta n_c = 0.3n_0$, $\Delta n_h = -0.3n_0$, $l_0 = 50\lambda_{dh}$, the grid spacing $\Delta x = 0.05\lambda_{dh}$, and time interval $\Delta t = 0.0001\omega_{pi}^{-1}$. We use negative amplitude perturbation in the hot electron fluid and positive amplitude perturbation in the cold electron fluid of the same magnitude to satisfy the quasi-neutrality condition at $t = 0$. The ions are considered to be stationary and uniform, hence no perturbation is given. The system length is taken as $L_x = 20,000\lambda_{dh}$. In simulation code, the time is normalized with inverse of ion plasma frequency, $\omega_{pi}^{-1} = \sqrt{\epsilon_0 m_i / n_0 e^2} = 2.33 \text{ ms}$, and space coordinate (x) is normalized with electron Debye length $\lambda_{dh} = \sqrt{\epsilon_0 T_h / n_0 e^2} = 51.3 \text{ m}$. Thus, the velocity automatically gets normalized with $\sqrt{T_h / m_i} = 138.4 \text{ km/s}$. The hot and cold electron plasma frequencies are respectively given by $\omega_{ph} = \sqrt{n_{h0} e^2 / \epsilon_0 m_e}$ and $\omega_{pc} = \sqrt{n_{c0} e^2 / \epsilon_0 m_e}$.

Initially, all fluids are stationary, and there is no electric field due to the quasi-neutrality in the system. However, the initial density perturbation produces a very small electric field due to the pressure gradients

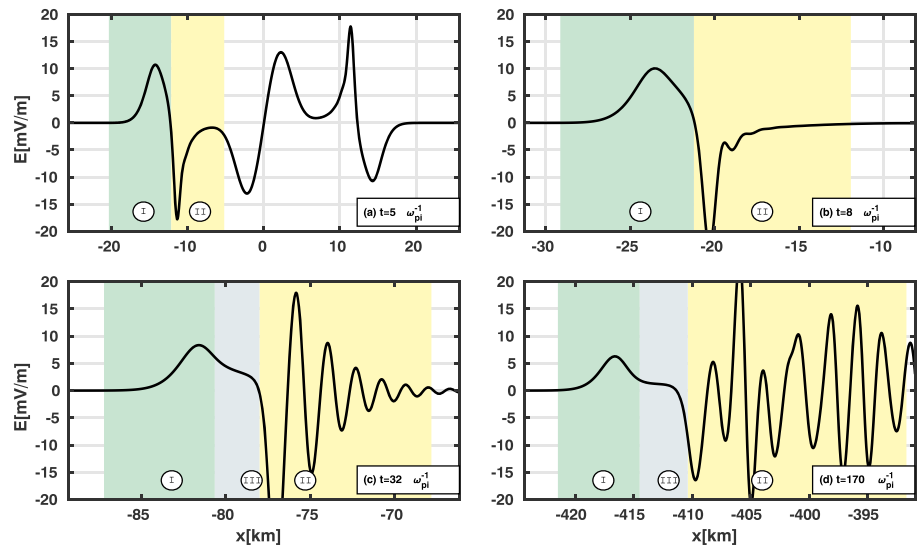


Figure 2. Figure shows various evolutionary stages in the course of formation of the electron acoustic double layer at different time instants (a) $\omega_{pi}t=5$, (b) $\omega_{pi}t=8$, (c) $\omega_{pi}t=32$, and (d) $\omega_{pi}t=170$.

developed through thermal motion of the electrons. This electric field oscillates and slowly evolves into the two identical oppositely propagating bipolar electric field pulse of EASWs as shown in Figure 2a. If we visualize them in the spacecraft reference frame, then the pulse in the positive x direction propagates along the magnetic field, whereas the pulse in the negative x direction propagates opposite to the magnetic field. As both pulses are indistinguishable, hereafter, we focus on the pulse that propagates opposite to the magnetic field. The trailing half cycle (i.e., in Region II) of this bipolar pulse steepens with time while moving ahead in the system, which is shown in Figure 2b. This steepening is identical to the classical steepening of acoustic waves which is discussed by Dillard et al. (2018). At later stage, the amplitude of the trailing wiggle increases and a shock-type structure is formed in Region II of Figure 2c. During this process, the shape of the leading wiggle (in Region I) also changes due to flattening of its backside as shown in Region III of Figure 2c. Further,

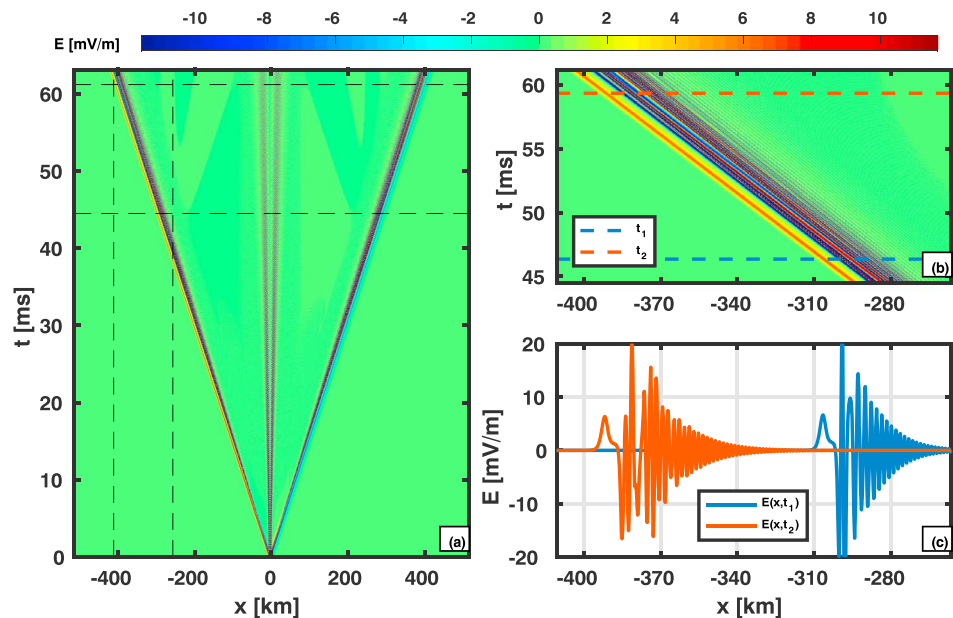


Figure 3. (a) Spatial and temporal variation of the electric field in the simulation. (b) The zoomed section marked by dashed black lines in panel (a). (c) Unipolar electric field structure associated with the electron acoustic double layer at two time instants (t_1 and t_2) marked by the two color lines in panel (b).

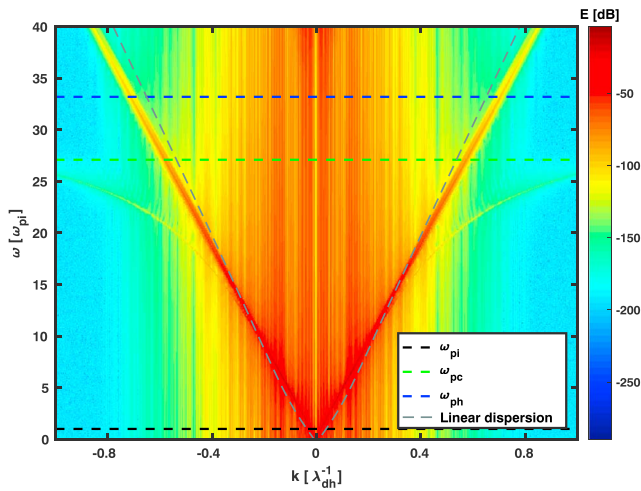


Figure 4. Dispersion plot obtained by fast Fourier transformation of electric field over spatial and temporal domain by taking data during $\omega_{pi}t = 0-170$.

the backside of this pulse completely flattens by achieving the uniform electric field, $E > 0$ in the Region III. The flatten edge in Region III together with the electric field pulse in Region I gives asymmetric shape to the pulse as shown in Figure 2d. This electric field pulse is associated with the net potential drop, which is similar to double layer. The animation (“ms01.gif”) of the evolution of the EADL pulse in the simulation is given in the supporting information. The physical mechanism responsible for transition of a symmetric EASW pulse to EADL is elaborated in section 4.

The spatial and temporal evolution of the EADLs in the system is shown in Figure 3a. The yellow (blue) band in this figure represents the evolution of EADL pulse propagating along the negative (positive) side of the x axis. These pulses have the same amplitudes but their electric fields have opposite polarities. The bunch of narrow bands followed by leading electric field pulse of EADL represents the evolution of the shock-type structure as shown in Figure 3b, which is zoomed portion of the region marked by dashed lines in Figure 3a. The growing distance between the EADL and shock-type structure with time indicates the dispersive nature of the shock. We examined the stability of the EADL pulse by plotting it

at two time instants $\omega_{pi}t_1 = 125$ and $\omega_{pi}t_2 = 165$, as shown in Figure 3c. This figure shows that the shape of EADL pulse remains the same while the shock amplitude decreases with time. To identify the mode associated with the double-layer pulses, we obtain the dispersion plot by taking the two-dimensional fast Fourier transformation of the electric field data during $\omega_{pi}t = 0-170$, which is shown in Figure 4. The black, green, and blue dashed lines in this figure indicate the plasma frequency of ions, cold electrons, and hot electrons, respectively. The slanted dashed gray lines are plotted from the linear dispersion of electron acoustic waves

$$1 - \sum_{s=c,h} \frac{\omega_{ps}^2}{\omega^2 - k^2 v_{ths}^2} = 0. \quad (9)$$

which is obtained by solving equations (1)-(4). In equation (9), $s = c, h$ is for cold and hot electron fluid, respectively. $\omega_{ps} = \sqrt{n_{s0} e^2 / \epsilon_0 m_s}$ and $v_{ths} = \sqrt{3T_s / m_s}$ are plasma frequency and thermal velocity of electrons, respectively. The dispersion curves from the simulation data and the theory shows their frequency extent above the ion plasma frequency indicating them as electron acoustic modes.

We validate the simulation results by comparing the electric field and potential profiles of the EADLs with the theory. In Figures 5a and 5c, we show the electric field profiles of the EADLs propagating along both positive and negative sides of the x axis. The electrostatic potential associated with these EADLs are shown in Figures 5b and 5d. We observe that the electric field and potential associated with the EADLs from theory and simulations are in agreement, which confirms that the evolved asymmetric electric field pulses in the simulation are EADLs. It is seen that the leading side of the EADL from the simulation is precisely matched with the theory; however, the trailing side of the EADL does not match due to the negative dip formed on its low potential side. The EADL profile in the simulation looks analogous to the structures reported by Vasko et al. (2017) using recent Van Allen Probe observations.

4. Mechanism for the Generation of EADLs

It is understood from the simulation that the symmetric bipolar electric field pulse of EASW transform to EADL through wave steepening. Basically, the steepening is an effect of the modulation of the plasma fluid in the vicinity of the electric field pulse. Hence, there must be some force that modulates some of the fluid elements in the vicinity of the electric field pulse. The electrostatic force will be the obvious cause in the present simulation. The electric field is time varying and has gradient over space. Hence, the electrostatic force will have low- and high-frequency components. The low-frequency component here is due to the ponderomotive force. The ponderomotive force experienced by charge particles in nonuniform oscillating electric field plays an important role in the modulation and stability of the ESWs (Kakad & Kakad, 2016; Lotekar et al., 2017). Hence in this section, we investigate the role of ponderomotive force.

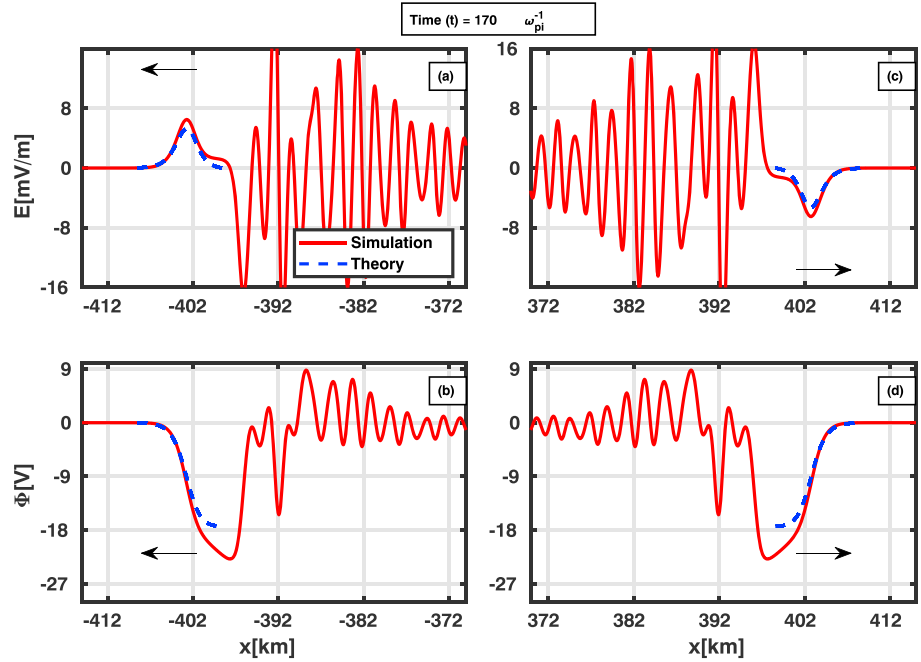


Figure 5. The electric field and electrostatic potential associated with the electron acoustic double layers obtained from the theory and simulation. The arrows in panel (a) and (b) show the electron acoustic double layer propagating in a direction opposite to the magnetic field, whereas (c) and (d) show the EADL propagating along the direction of magnetic field.

The ponderomotive force is given by

$$F_p = -\frac{1}{4} \frac{e^2}{m_s \Omega^2} \frac{\partial}{\partial x} |E|^2 \quad (10)$$

Here, Ω is the oscillating frequency of the electric field, and it can be calculated from the simulation as follows (Kakad & Kakad, 2016; Kakad et al., 2017; Lotekar et al., 2017),

$$\Omega_{ps}^2 = \frac{1}{4} \frac{U}{KE_s} \omega_s^2 \quad (11)$$

where $KE_s = n_s m_s v_s^2 / 2$ and ω_{ps} are the kinetic energy density and plasma frequency of the species s , respectively. The electrostatic energy density $\epsilon_0 E^2 / 2$ is denoted by U . Using equations (10) and (11), we obtained the magnitude and direction of the ponderomotive force acting on the cold and hot electron fluids at each grid point in the simulation. It is found that the ponderomotive force acting on the cold fluid is greater than the ponderomotive force acting on the hot fluid, whereas the direction of the ponderomotive force acting on both cold and hot electrons is the same (See panel a of the animation “ms02.gif” in the supporting information). The ponderomotive force acting spatially on the cold electron fluid at different stages of evolution is shown using arrows in Figure 6. In this figure, the magnitude of the ponderomotive force on the grid points is scaled with the arrow length for better visibility. The ponderomotive force associated with the blue (red) arrows is scaled such that 1 km $\approx 3.7 \times 10^{-20}$ N (1 km $\approx 3.7 \times 10^{-19}$ N).

During the initial time, the ponderomotive force acting on the electron fluid around the center of the system has higher magnitude due to large spatial gradients in the electric field. As mentioned earlier, the force acting on cold electrons is larger in magnitude as compared to that on hot electrons. The direction of ponderomotive force is such that it pushes the cold electron fluids in the region of weaker electric fields. The action of ponderomotive force leads to the formation of two humps (dips) in the cold (hot) electron density around both sides of the center of the system. It give rise to localized net charge density, which is manifested as two indistinguishable oppositely propagating bipolar electric field pulses propagating away from the center of simulation system as shown in Figure 6a (See panel b and c of animation “ms02.gif” in the supporting information). These bipolar electric field pulses evolve with time. Further, we discuss the modulation of the bipolar electric field pulse propagating toward the negative x direction as shown in Figure 6b.

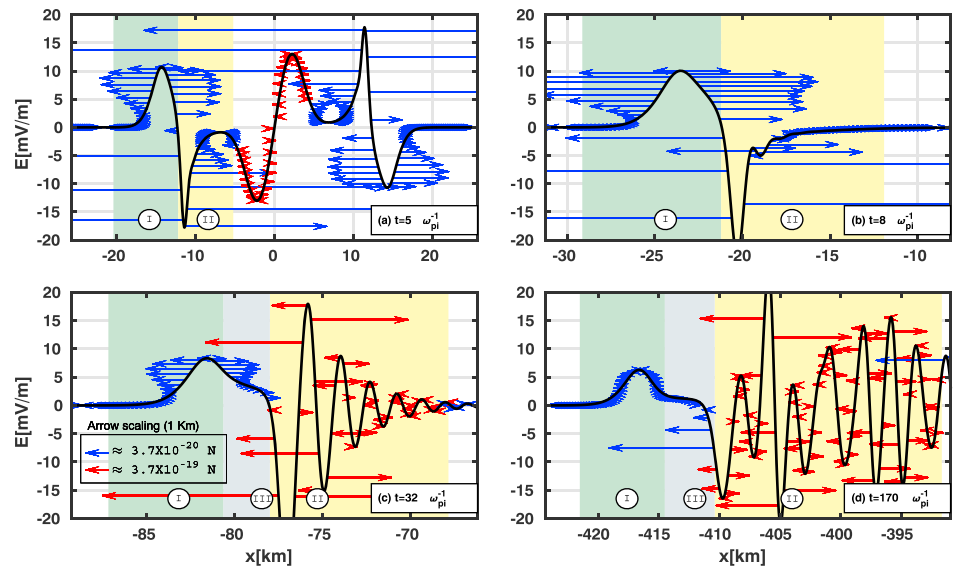


Figure 6. A spatially varying ponderomotive force over the electric field structures in the course of formation of electron acoustic double layers at different time instants (a) $\omega_{pi}t=5$, (b) $\omega_{pi}t=8$, (c) $\omega_{pi}t=32$, and (d) $\omega_{pi}t=170$. The length of the arrows is scaled with the ponderomotive force magnitude. The red and blue arrows are scaled with different magnitudes of ponderomotive force.

A careful scrutinizing of Figure 6b shows that the ponderomotive force acting on the inner edge of the lower half (–ve hump) and upper half (+ve hump) of the bipolar electric field is strongly imbalanced. In the bottom side, large ponderomotive force compresses the electron fluid elements toward the leftward direction. This shortens the wavelength of some of the oscillating electron fluid elements below the Debye length ($k^2 \lambda_{dh}^2 > 1$). Hence, due to the dispersive effect, these electron fluid elements decelerate and start lagging behind (Kakad et al., 2013; Lotekar et al., 2016, 2017). As a result, in Region II the accumulation of electron fluid elements occur and leads to the formation of large-magnitude negative polarity electric field pulse (see Region II in Figure 6c). This process continues and the shock-type structure forms (see Region II in Figure 6d).

During the process of evolution, the inner edge of the first half (+ve hump) of bipolar electric field, where ponderomotive force act in the rightward direction (see Figure 6b) gets modulated to form Region III (see Figure 6c). The sharp gradient electric field in Region II results in a stronger ponderomotive force in the leftward and rightward direction as shown in Figure 6c. The shock-type structure in Region II acts as a barrier for the electron fluid coming from Region III. The propagation of the shock-type structure is dispersive; therefore, the distance between the shock-type structure and leading electric field pulse increases with time. This is conspicuous in Region III of Figure 6d. In Region III, the fluid continuously spreads to maintain the constant charge density, and electric field attains the uniform value by forming a plateau. This plateau and the attached leading electric field pulse forms the EADL, which is perceptible in Figure 6d. After formation of the EADL, there is no further change in its shape/size as the ponderomotive force in Region III is significantly weak to cause any further modulation in the electron fluid. This helps to maintain the shape of the EADL pulse to be stable for a longer time during its propagation.

5. Concluding Remarks

In this paper, we have addressed the generation mechanism and the formation process of the EADLs observed by Van Allen Probe in the Earth’s inner magnetosphere. First, the nonlinear fluid model is formulated based on the EADLs observations reported by Vasko et al. (2017). The amplitude and velocity of observed electric field structures are found to be in good agreement with the nonlinear theory. The nonlinear theory characterizes these structures as slow refractive EADLs but found to be incapable of modeling the evolution of EADLs. Further, we carried out the fluid simulation of the formation of EADLs for the observed plasma parameters in the inner magnetosphere. Our simulation shows that a localized enhancement of the cold electron population and depletion in the hot electron density can generate the EADLs. The amplitude

and velocity of the EADLs generated in the simulation are in agreement with the observed ones. In this paper, we have discussed the formation of EADLs for one set of ambient parameters. However, by varying cold electron density and temperature in the simulation, one can reproduce the entire characteristic range of the observed EADLs.

In general, two parallel layers of opposite electrical charges form a double layer in the plasma. However, this is not the case in the formation of EADLs in the present study. Our simulation shows that the ponderomotive force acting on the cold and hot electron fluid plays a constitutive part in the transformation of bipolar electric field pulse to the EADL in the plasma. The negative and positive amplitude perturbations in the equilibrium electron densities generate the unstable bipolar electric field pulses, which later evolve into the EADLs and shock-type structure. In order to generate the symmetric pulse, the electron density at the trailing edge (shock-side) of the DL must reach to the equilibrium value by expelling the fluid to the shock area. However, the stronger ponderomotive force on the shock front restricts the motion of this flow at the trailing edge of the EADL. This leads to the formation of plateau of the uniform electron density (which is above the equilibrium electron density due to the accumulation of electrons) between the EADL and the shock, which gives the asymmetric shape to the pulse. The ponderomotive force on the plateau is almost zero; therefore, the shape of the EADL does not distort further, which is evident in the simulation as well. This study provides the insights on the generation mechanism of the EADLs in the Earth's inner magnetosphere.

Acknowledgments

The model computations were performed on the High Performance Computing System at the Indian Institute of Geomagnetism, India. The observational data presented in Table 1 of the manuscript have been taken from Vasko et al. (2017).

References

- Cattell, C., Dombeck, J., Wygant, J., Drake, J. F., Swisdak, M., Goldstein, M. L., et al. (2005). Cluster observations of electron holes in association with magnetotail reconnection and comparison to simulations. *Journal of Geophysical Research*, *110*, A01211. <https://doi.org/10.1029/2004JA010519>
- Dillard, C. S., Vasko, I. Y., Mozer, F. S., Agapitov, O. V., & Bonnell, J. W. (2018). Electron-acoustic solitary waves in the Earth's inner magnetosphere. *Physics of Plasmas*, *25*(2), 22905. <https://doi.org/10.1063/1.5007907>
- Ergun, R. E., Carlson, C. W., McFadden, J. P., Mozer, F. S., Delory, G. T., Peria, W., et al. (1998). FAST satellite observations of large-amplitude solitary structures. *Geophysical Research Letters*, *25*, 2041–2044. <https://doi.org/10.1029/98GL00636>
- Ergun, R. E., Goodrich, K. A., Stawarz, J. E., Andersson, L., & Angelopoulos, V. (2015). Large amplitude electric fields associated with bursty bulk flow braking in the Earth's plasma sheet. *Journal of Geophysical Research: Space Physics*, *120*, 1832–1844. <https://doi.org/10.1002/2014ja020165>
- Fu, X., Cowee, M. M., Gary, S. P., & Winske, D. (2016). On the generation of double layers from ion-and electron-acoustic instabilities. *Physics of Plasmas*, *23*(3), 32308. <https://doi.org/10.1063/1.4943881>
- Funsten, H. O., Skoug, R. M., Guthrie, A. A., MacDonald, E. A., Baldonado, J. R., Harper, R. W., et al. (2013). Helium, oxygen, proton, and electron (HOPE) mass spectrometer for the radiation belt storm probes mission. *Space Science Reviews*, *179*, 423–484. <https://doi.org/10.1007/978-1-4899-7433-4?urlscore=13>
- Kakad, A., & Kakad, B. (2016). Ponderomotive processes as proxies for breaking of ion acoustic solitary waves. *Physics of Plasmas*, *23*(12), 122101. <https://doi.org/10.1063/1.4968842>
- Kakad, A., Kakad, B., Anekallu, C., Lakhina, G., Omura, Y., & Fazakerley A. (2016). Slow electrostatic solitary waves in Earth's plasma sheet boundary layer. *Journal of Geophysical Research: Space Physics*, *121*, 4452–4465. <https://doi.org/10.1002/2016JA022365>
- Kakad, A., Kakad, B., Lotekar, A., & Lakhina, G. S. (2019). Role of ion thermal velocity in the formation and dynamics of electrostatic solitary waves in plasmas. *Physics of Plasmas*, *26*(4), 42112.
- Kakad, B., Kakad, A., & Omura, Y. (2014). Nonlinear evolution of ion acoustic solitary waves in space plasmas: Fluid and particle in cell simulations. *Journal of Geophysical Research: Space Physics*, *119*, 5589–5599. <https://doi.org/10.1002/2014ja019798>
- Kakad, B., Kakad, A., & Omura, Y. (2017). Particle trapping and ponderomotive processes during breaking of ion acoustic waves in plasmas. *Physics of Plasmas*, *24*(10), 102122. <https://doi.org/10.1063/1.4986030>
- Kakad, A., Omura, Y., & Kakad, B. (2013). Experimental evidence of ion acoustic soliton chain formation and validation of nonlinear fluid theory. *Physics of Plasmas*, *20*(6), 13. <https://doi.org/10.1063/1.4810794>
- Lotekar, A., Kakad, A., & Kakad, B. (2016). Fluid simulation of dispersive and nondispersive ion acoustic waves in the presence of superthermal electrons. *Physics of Plasmas*, *23*(10), 102108. <https://doi.org/10.1063/1.4964478>
- Lotekar, A., Kakad, A., & Kakad, B. (2017). Generation of ion acoustic solitary waves through wave breaking in superthermal plasmas. *Physics of Plasmas*, *24*(10), 102127. <https://doi.org/10.1063/1.4991467>
- Malaspina, D., Andersson, L., Ergun, R. E., Wygant, J. R., Bonnell, J. W., Kletzing, C., et al. (2014). Nonlinear electric field structures in the inner magnetosphere. *Geophysical Research Letters*, *41*, 5693–5701. <https://doi.org/10.1002/2014GL061109>
- Malaspina, D. M., Ukhorskiy, A., Chu, X., & Wygant, J. (2018). A census of plasma waves and structures associated with an injection front in the inner magnetosphere. *Journal of Geophysical Research: Space Physics*, *123*, 2566–2587. <https://doi.org/10.1002/2017JA025005>
- Matsumoto, H., Kojima, H., Miyatake, T., Omura, Y., Okada, M., Nagano, I., et al. (1994). Electrostatic solitary waves (ESW) in the magnetotail: BEN wave forms observed by GEOTAIL. *Geophysical Research Letters*, *25*, 2915–2918. <https://doi.org/10.1029/94GL01284>
- Mozer, F. S., Agapitov, O. V., Artemyev, A., Drake, J. F., Krasnoselskikh, V., Lejosne, S., & Vasko, I. (2015). Time domain structures: What and where they are, what they do, and how they are made. *Geophysical Research Letters*, *42*, 3627–3638. <https://doi.org/10.1002/2015GL063946>
- Olivier, C. P., Maharaj, S. K., & Bharuthram, R. (2015). Ion-acoustic solitons, double layers and supersolitons in a plasma with two ion- and two electron species. *Physics of Plasmas*, *22*, 82312. <https://doi.org/10.1063/1.4928884>
- Sagdeev, R. Z. (1966). Cooperative phenomena and shock waves in collisionless plasmas. *Reviews of modern plasma physics*, *4*, 23–91.
- Vasko, I. Y., Agapitov, O. V., Mozer, F. S., Bonnell, J. W., Artemyev, A. V., Krasnoselskikh, V. V., et al. (2017). Electron-acoustic solitons and double layers in the inner magnetosphere. *Geophysical Research Letters*, *44*, 4575–4583. <https://doi.org/10.1002/2017GL074026>

- Vasko, I. Y., Agapitov, O. V., Mozer, F. S., Bonnell, J. W., Artemyev, A. V., Krasnoselskikh, V. V., & Tong, Y. (2018). Electrostatic steepening of whistler waves. *Phys Revista de Letras*, *120*(19), 195101. <https://doi.org/10.1103/PhysRevLett.120.195101>
- Watanabe, K., & Taniuti, T. (1977). Electron-acoustic mode in plasma of two-temperature electrons. *Journal of the Physical Society of Japan*, *43*(5), 1819–1820. <https://doi.org/10.1143/JPSJ.43.1819>